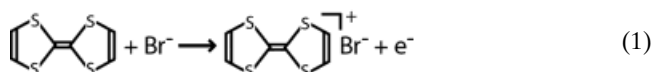


- [11] G. U. Sumanasekera, C. K. W. Adu, S. Fang, P. C. Eklund, *Phys. Rev. Lett.* **2000**, *85*, 1096.
 [12] W. B. Choi, Y. H. Lee, N. S. Lee, J. H. Kang, S. H. Park, H. Y. Kim, D. S. Chung, S. M. Lee, S. Y. Chung, J. M. Kim, *Jpn. J. Appl. Phys.* **2000**, *39*, 2560.
 [13] H. Murakami, M. Hirakawa, C. Tanaka, H. Yamakawa, *Appl. Phys. Lett.* **2000**, *76*, 1776.
 [14] X. Xu, G. R. Brandes, *Appl. Phys. Lett.* **1999**, *74*, 2549.
 [15] Y. M. Shin, H. J. Jeong, Y. H. Lee, unpublished.
 [16] Y. C. Choi, Y. M. Shin, S. C. Lim, D. J. Bae, Y. H. Lee, B. S. Lee, *J. Appl. Phys.* **2000**, *88*, 4898.
 [17] Y. C. Choi, Y. M. Shin, D. J. Bae, S. C. Lim, Y. H. Lee, B. S. Lee, *Diamond Relat. Mater.* **2001**, *10*, 1457.
 [18] P. R. Schwoebel, I. Brodie, *J. Vac. Sci. Technol. B* **1995**, *13*, 1391.
 [19] J. M. Bonard, J. P. Salvetat, T. Stockli, W. A. de Heer, L. Forro, A. Chate-lain, *Appl. Phys. Lett.* **1998**, *73*, 918.
 [20] P. G. Collins, A. Zettl, *Phys. Rev. B* **1997**, *55*, 9391.
 [21] Y. C. Choi, Y. M. Shin, Y. H. Lee, B. S. Lee, G.-S. Park, W. B. Choi, N. S. Lee, J. M. Kim, *Appl. Phys. Lett.* **2000**, *76*, 2367.
 [22] X. Y. Zhu, S. M. Lee, Y. H. Lee, T. Frauenheim, *Phys. Rev. Lett.* **2000**, *85*, 2757.

Size-Selective Growth of Nanoscale Tetrathiafulvalene Bromide Crystallites on Platinum Particles**

By Fred Favier, Hongtao Liu, and Reginald M. Penner*

We describe the preparation of long (>1.0 μm) nanocrystallites of an electronically conductive organic charge transfer salt, tetrathiafulvalene bromide, which are narrowly dispersed in diameter. Our method involves the size-selective electrocrystallization of this salt on platinum catalyst particles supported on a graphite surface. These platinum particles, ranging in diameter from 70 nm to 1.3 μm , were prepared by electrodeposition.^[1–3] The electrocrystallization of tetrathiafulvalene bromide ((TTF)Br_x) from a dimethyl acetamide (DMAC) solution was then carried out at this nanostructured surface. (TTF)Br_x nanocrystals having widths in the range from 30 nm to 600 nm and aspect ratios of 20 or more were formed at the platinum nanoparticles on these surfaces by the electrochemical oxidation of tetrathiafulvalene (TTF) in bromide-containing electrolyte according to the reaction:^[4]



[*] Prof. R. M. Penner, Dr. H. Liu
 Institute for Surface and Interface Science, Department of Chemistry
 University of California, Irvine
 Irvine, CA 92679-2025 (USA)
 E-mail: rmpenner@uci.edu
 Dr. F. Favier
 UMR 5072 CNRS-UMII
 F-34095 Montpellier (France)

[**] This work was funded by the National Science Foundation (#DMR-9876479) and the Petroleum Research Fund of the American Chemical Society (#33751-AC5). R.P. acknowledges the financial support of the A.P. Sloan Foundation Fellowship, and the Camille and Henry Dreyfus Foundation. F.F. acknowledges funding through NATO. Finally, donations of graphite by Dr. Art Moore of Advanced Ceramics are gratefully acknowledged.

Under the conditions employed in this study, the product of this oxidation was the non-stoichiometric salt (TTF)Br_x where *x* is close to 0.76.^[5] The widths of the (TTF)Br_{0.76} crystallites (henceforth, (TTF)Br) were directly proportional to the diameter of the platinum particles on which they nucleated and grew. Specifically, the widths of (TTF)Br crystallites were 40–45 % of the platinum particle diameter over the entire range indicated above. We believe these observations constitute the first clear demonstration that a nanomaterial can be obtained size-selectively by electrodeposition using size-selected metal particles as electrocatalysts.

Crystalline (TTF)Br is a highly anisotropic material both in terms of its reactivity (with respect to growth and dissolution), and its electrical conductivity. This anisotropy is a manifestation of its crystal structure in which π -stacks of TTF⁺ electron acceptors—arrayed along the *c*-axis of the crystal—are arranged in parallel to an equal number of (incomplete) rows of Br⁻ electron donors.^[5] In (TTF)Br electrons are delocalized along these TTF⁺ stacks and the crystal is therefore conductive along the *c*-axis. The conductivity of single crystals in the direction perpendicular to the stacking direction is much lower. During electrocrystallization, (TTF)Br crystallites grow rapidly in the direction of the *c*-axis with the result that long, narrow crystallites are produced even at a smooth metal electrode surface.^[6,7] However, in all previous studies, the width of these crystallites has been uncontrolled.

We investigated the growth of (TTF)Br crystallites at graphite surfaces covered with platinum nanoparticles ranging in diameter from 70 nm to 1.3 μm . These nanoparticles were prepared using the “slow growth” electrodeposition technique as previously described.^[1,2] Briefly, in an aqueous plating solution of 1 mM H₂PtCl₆ (Aldrich, 99.99 %) and 0.1 M HCl (Fisher, >99.95 %), a sequence of two voltage pulses was applied: The first or nucleation pulse was 5 ms at -0.4 V vs. saturated calomel electrode (SCE) and it was followed by a growth pulse of +0.15 V vs. SCE, which had a duration of between 20 and 120 min. In order to avoid the “electroless” deposition of platinum in this electrolyte,^[3] the graphite electrode was anodically protected at +0.5 V vs. SCE during exposure to the electrolyte.^[3]

The resulting platinum particle modified graphite electrode was used as the working electrode in a one-compartment glass cell for the (TTF)Br electrocrystallization. The counter electrode was a 1.0 cm² platinum foil and a 1 mm diameter Pt wire was employed as a pseudo-reference electrode. A solution containing 0.1 M tetrabutylammonium bromide (Aldrich, 99 %) and 5 mM TTF (Aldrich, 99 %) in DMAC (Aldrich, 99.8 % anhydrous) was anaerobically transferred to the cell. (TTF)Br crystals were obtained using a train of between 1 and 15 pulses of 0.2 s at +650 mV vs. Pt. Platinum particle growth and TTF(Br) electrocrystallization were carried out under computer control using an EG&G 270M potentiostat.

Shown in Figure 1 are scanning electron micrographs (SEMs) of platinum particles before and after the electrocrystallization of (TTF)Br crystallites. These platinum particles, prepared using the “slow growth” protocol described above

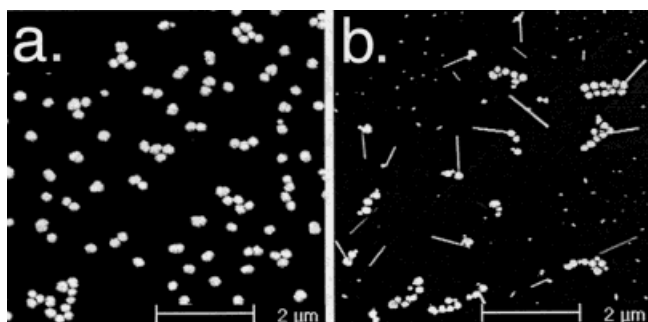


Fig. 1. SEM images of HOPG electrode surfaces following the electrodeposition of platinum nanoparticles (a) and the electrocrystallization of tetrathiafulvalene bromide on a platinum nanoparticle-covered graphite surface (b).

(Fig. 1a), were narrowly dispersed in diameter, and somewhat aggregated on the graphite surface. Following the electrocrystallization of (TTF)Br (Fig. 1b) a single (TTF)Br crystallite was observed at most of the platinum particle aggregates on the surface. Also shown in Figure 1b, around the periphery of this image, are smaller (TTF)Br crystallites that have nucleated on the graphite surface. As compared with the (TTF)Br crystallites that have nucleated on platinum particles, those that have nucleated on the graphite surface are smaller in volume by a factor of 100. This disparity suggests that platinum particles are efficient catalysts for the electrocrystallization of (TTF)Br. A closer inspection of Figure 1b reveals that the (TTF)Br crystallites that have nucleated on the graphite surface have not done so uniformly across the graphite surface. Instead, an “exclusion zone” within which no (TTF)Br nuclei are seen is observed within several radii of platinum particles. The existence of this zone is highlighted for one cluster of platinum particles in Figure 2. One possible origin for this exclusion zone is the consumption of physisorbed TTF molecules (presumably required for the nucleation of (TTF)Br) by platinum particles on the surface. If physisorbed TTF is consumed by platinum particles on the

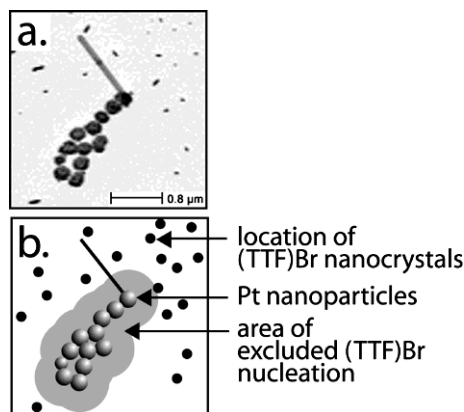


Fig. 2. a) An ensemble of platinum nanoparticles following the electrocrystallization of (TTF)Br; a single (TTF)Br crystallite has nucleated on one of the particles within this ensemble. (TTF)Br crystallites are not observed immediately adjacent to platinum particles on the surface. b) Schematic representation of the “exclusion zone” (in gray) surrounding platinum catalyst particles for the ensemble shown in (a). The positions of (TTF)Br crystallites on the graphite surface are marked by black dots.

surface, and these TTF molecules possess some lateral mobility, then the graphite surface near each platinum particle will be depleted of physisorbed TTF and the probability of (TTF)Br nucleation within this zone will be reduced.

The central point of this paper is that the widths of (TTF)Br crystallites are directly proportional to the diameter of the platinum catalyst particles. Shown in Figure 3, for example, are SEM images that show the (TTF)Br crystallites obtained from platinum particles having four different diameters span-

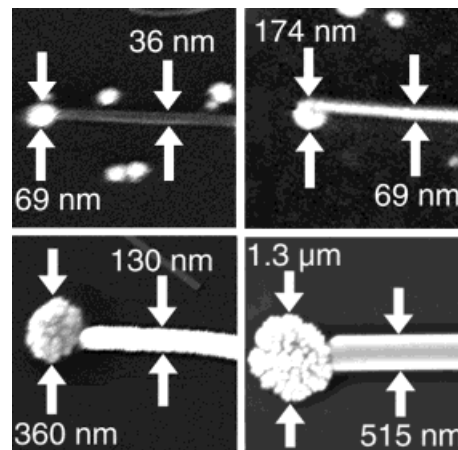


Fig. 3. SEM images of four (TTF)Br crystallites and the platinum nanoparticles on which they nucleated.

ning more than an order of magnitude. A correlation between the diameter of the platinum catalyst particle, and the width of the (TTF)Br crystallite is obvious from these images, and it is clear that in each case the width of the (TTF)Br crystallite is 40–45 % of the diameter of the platinum particle. The size-selective growth of a single (TTF)Br crystallite is observed on these platinum particles even though, as the SEM images clearly show, these particles are polycrystalline.

An analysis of 107 (TTF)Br crystallites obtained in many separate experiments is shown in Figure 4. A clear linear relationship between the platinum particle diameter and the width of the (TTF)Br crystallite is seen for (TTF)Br crystal-

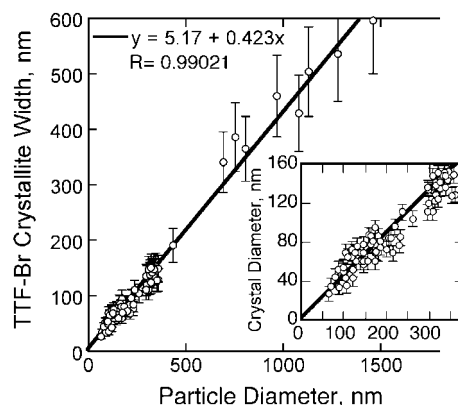


Fig. 4. Plot of (TTF)Br crystallite width as a function of the diameter of the platinum particle on which nucleation occurred for 107 crystallites. The error bars in this plot estimate the precision with which the dimensions of particles and crystallites could be measured.

lites ranging in diameter from 25 nm to 600 nm. Remarkably, the correlation coefficient (R)^[8] for these data over this entire range is 0.99. The slope of this plot is 0.423. This means that the width of a (TTF)Br crystallite is, on average, 0.423 of the diameter of the platinum particle on which it nucleates and grows. This ratio is not a fundamental materials property of the Pt/(TTF)Br system. Instead, the width of the (TTF)Br crystallite obtained from platinum particles of a particular diameter depended both on the oxidation potential employed for (TTF)Br deposition and on the deposition time. More positive oxidation potentials or longer depositions produced (TTF)Br crystallites that were larger than 0.42 of the platinum particles diameter, and more negative deposition potentials or shorter deposition durations yielded smaller values for this ratio. The data of Figure 4 shows that for a specific set of deposition conditions, the proportionality between TTF(Br) crystallite width and platinum particle diameter is maintained over a wide range.

Two factors operating in concert are likely responsible for this size-selective electrocrystallization. First, as already mentioned, the conductivity of the (TTF)Br crystal is much higher along the c -axis direction than in the directions perpendicular to it. Qualitatively, this means that the potential present along the “sides” of the (TTF)Br crystallites can be lower than the potential present at the c -terminus of the crystal. A second factor relates to the kinetics of crystal growth, which are much faster in the c -direction than in the directions perpendicular to it. At present, we have no data that sheds any light on the relative importance of these two causal factors.

The data of Figure 4 suggests that populations of (TTF)Br crystallites that are narrowly dispersed in width could be obtained by electrodeposition on dimensionally uniform platinum nanoparticles. This is indeed the case. Figure 5 shows histograms of platinum nanoparticles, and the (TTF)Br nanocrystallites obtained from them, for two separate growth experiments. The platinum particles in these experiments with mean diameters of 80 nm and 140 nm were prepared using “slow growth” as previously described^[1,2] and were narrowly dispersed in diameter. The synthesis of (TTF)Br crystallites on these two surfaces yielded populations of crystallites char-

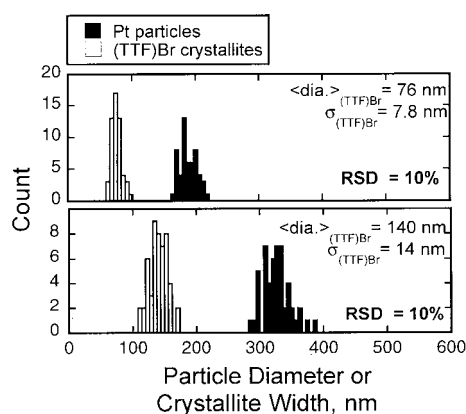


Fig. 5. Size distributions for the platinum particles (■) and the (TTF)Br crystallites (□) deposited in two representative experiments.

acterized by a relative standard deviation of the crystallite width, RSD_{width} , of 10 %.

The data presented here support the following conclusions:

- At graphite electrode surfaces, the electrosynthesis of (TTF)Br is catalyzed by platinum nanoparticles.
- Only 15–25 % of the platinum nanoparticles on the surface are involved in TTF(Br) crystallization. In cases where platinum particles were aggregated on the surface, each particle aggregate produced at most one (TTF)Br crystallite.
- (TTF)Br crystallites that nucleate and grow on platinum particles exhibit widths that are linearly related to the diameter of the platinum particles on which they grow. This linear scaling of the (TTF)Br width was observed for platinum particles ranging in diameter from 70 nm to 1.3 μm and (TTF)Br widths of 30 nm to 600 nm. The deposition conditions employed here yielded a ratio of (TTF)Br crystallite width to platinum particle diameter of 0.423. The aspect ratios of these crystallites (length/width) were in the range from 5 to 30.
- Populations of long (TTF)Br crystallites having a predetermined width can be prepared by electrodeposition onto surfaces covered with size-monodispersed platinum catalyst particles (also prepared by “slow growth” electrodeposition).

Experimental

Electrochemical Measurements: Pt particles were electrodeposited on freshly cleaved highly oriented pyrolytic graphite (HOPG) samples using the slow growth method as previously described [1,2]. Briefly, 50 nm to 1.5 μm Pt particles were prepared from an N_2 -sparged aqueous plating solution containing 1 mM H_2PtCl_6 (Aldrich, 99.99 %) and 0.1 M HCl (Fisher, >99.95 %). This plating solution was prepared using Barnstead Nanopure deionized water ($\rho > 17.8 \text{ M}\Omega$). “Slow growth” electrodeposition was carried out by applying a 5 ms nucleation pulse of -4.0 V vs. SCE to the working electrode, followed immediately by a growth pulse of $+0.150 \text{ V}$ vs. SCE lasting between 20 and 120 min. A potential of $+0.5 \text{ V}$ vs. SCE was applied during the immersion and removal of the working electrode into the platinum plating solution to prevent the “electroless deposition” of platinum [3].

The resulting platinum particle-modified HOPG surface was used as the working electrode in a one-compartment closed glass cell for the (TTF)Br_x ($x = 0.74\text{--}0.79$) electrocrystallization. The counter electrode was a 1.0 cm^2 Pt foil and a platinum wire pseudo-reference electrode was employed. A solution containing 0.1 M tetrabutylammonium bromide (Aldrich, 99 %) and 5 mM TTF (Aldrich, 99 %) in DMAC (Aldrich, 99.8 % anhydrous) was anaerobically transferred into the one-compartment glass cell. (TTF)Br_x crystals were synthesized by applying a series of 1 to 15 voltage pulses to the working electrode. These pulses had a duration of 0.2 s and an amplitude of $+650 \text{ mV}$ vs. Pt. All these electrolyses were performed using a computer-controlled EG&G 270M potentiostat.

Electron Microscopy: Samples to be examined using SEM were mounted on an aluminum SEM stub using adhesive carbon dots (Ted Pella, Inc) and dried in a vacuum desiccator for 4 h. SEM was carried out using a Philips Model XL-30FEG operating at 15–30 keV. Crystallite diameters were manually determined from high-magnification SEM images.

Received: April 25, 2001
Final version: June 19, 2001

- [1] H. Liu, R. M. Penner, *J. Phys. Chem. B* **2000**, *104*, 9131.
[2] H. Liu, F. Favier, K. Ng, M. P. Zach, R. M. Penner, *Electrochim. Acta*, in press.
[3] J. V. Zoval, J. Lee, S. Gorer, R. M. Penner, *J. Phys. Chem. B* **1998**, *102*, 1166.

- [4] F. B. Kaufman, E. M. Engler, D. C. Green, J. Q. Chambers, *J. Am. Chem. Soc.* **1976**, *98*, 1596.
 [5] B. A. Scott, S. J. La Place, T. B. Torrance, B. D. Silverman, B. Welber, *J. Am. Chem. Soc.* **1977**, *99*, 6631.
 [6] C. Gurtner, M. J. Sailor, A. S. Katz, R. C. Dynes, *J. Phys. Chem. B* **1998**, *102*, 1599.
 [7] C. Gurtner, A. W. Wun, M. Sailor, *Angew. Chem. Int. Ed.* **1999**, *38*, 1966.
 [8] R is the square root of the coefficient of determination, often used to express the degree to which a regression line predicts the actual Y vs. X data. A formal definition of R is:

$$R = \frac{S_{XY}}{\sqrt{S_X S_Y}} \quad (2)$$

where: $S_{XY} = \Sigma(X - \langle X \rangle)(Y - \langle Y \rangle)$; $S_X = \Sigma(X - \langle X \rangle)^2$; $S_Y = \Sigma(Y - \langle Y \rangle)^2$. See, for example: L. Sachs, *Applied statistics: A Handbook of Techniques*, 2nd ed. (Translator: Z. Reynarowych), Springer, New York **1984**.

One-Step, Micrometer-Scale Organization of Nano- and Mesoparticles Using Holographic Photopolymerization: A Generic Technique**

By Richard A. Vaia,* Cindi L. Dennis, Lalgudi V. Natarajan, Vincent P. Tondiglia, David W. Tomlin, and Timothy J. Bunning*

The promise of faster computation, denser memories, ultra-small machines, and the establishment of a robust interface between artificial and biological devices has spurred substantial worldwide investment in nanotechnology.^[1] Critical to the success of nanotechnology is not just the development of new nanoscale (1–100 nm) building-blocks (material units with unique physical properties)^[2] but also the development of cost-effective approaches amenable to rapid, large scale (0.01–1 m) assembly in multiple dimensions. Integration over meso (100–1000 nm) and microscale (1–100 μm) dimensions of function is necessary in order to combine utilities and establish a connection with the external environment. The expansion beyond conventional semiconductor processing approaches and development of routes that enable precise, three-dimensional patterning of soft matter, including polymers and biological materials, is of special interest. Controlled, spatially defined incorporation of a variable sized particle (metallic, glassy, polymeric, or inorganic) leads to the promise of complex, functional systems, which can be exploited due to anisotropy of function.

The ability to direct the spatial distribution of particles in soft matter with two- and three-dimensional control is currently the focus of many research groups. A number of processes are presently being examined, including micro-contact printing,^[3] colloidal crystal processing,^[4] e-beam and X-ray lithography,^[5] pattern-directed dewetting,^[6] polyelectrolyte deposition,^[7] surfactant (micelle) directed processing,^[8] block copolymer templating,^[9] dip pen lithography,^[10] deoxyribonucleic acid (DNA) and enzymatic directed assembly,^[11] and direct unit placement with scanning tunneling microscopy (STM) and atomic force microscopy (AFM).^[12] Many of these approaches follow conventional integrated circuit processing methodologies, combining previously developed thin-film deposition techniques, which enable one-dimensional compositional control normal to a surface, with two-dimensional patterning concepts. These approaches create a sequential methodology to build compositional patterns on a surface. Each approach to patterning has specific advantages and disadvantages that are dependent on the material components, substrate, geometry, size, available processing time, and functional response desired. However, none of these techniques enable true one-step (non-sequential) patterning of generic particles (regardless of its shape, size, and composition) into complex patterns on multiple length scales and arbitrary orientation.

An alternative approach discussed here that has the potential to approach these generic objectives is holographic photopolymerization. Interference of two or more coherent laser beams within a photo-reactive monomer syrup results in a periodic intensity distribution that initiates a self-similar periodic polymerization process. A higher intensity results in a higher local free-radical concentration, which in turn results in a locally faster polymerization rate. This rate anisotropy causes a spatial distribution of high molecular weight polymer to develop, which changes over time. The intensity of the two writing beams and relative reactivity of different monomers can be used to modulate the temporal evolution of the anisotropy.

Utilization of this process was first demonstrated in the early 1970s in pure polymer films as an effective means to generate periodic refractive index gratings normal to the surface of a film.^[13] These highly colored films (due to diffraction) are now the commercial basis for DuPont's holographic component product line.^[14] This approach has been extended by adding a non-reactive fluid component (liquid crystal, LC) to the photoreactive syrup.^[15–17] The propensity of phase separation in mixtures of high molecular weight polymers and low molar mass liquid crystals in sufficient concentration combined with the spatial and temporal anisotropy of holographic polymerization results in the periodic phase separation of nanoscale-sized LC domains. These small domains are spatially separated by crosslinked polymer regions on a periodicity defined by the holography process. These periodic, sub-micrometer Bragg gratings exhibit high diffraction efficiencies that can be modulated using applied external electric fields. The gratings are formed in one step (seconds), on large areas

[*] Dr. T. J. Bunning, Dr. R. A. Vaia, C. L. Dennis
 Air Force Research Laboratory, Materials and Manufacturing Directorate
 AFRL/MLPJ
 3005 P. St., Ste. 1, WPAFB, OH 45433 (USA)
 E-mail: Timothy.Bunning@afml.af.mil
 Dr. L. V. Natarajan, V. P. Tondiglia
 Science Applications International Corporation
 4031 Colonel Glenn Highway, Dayton, OH 45431 (USA)
 Dr. D. W. Tomlin
 Technical Management Concepts, Inc.
 Beavercreek, OH 45432 (USA)

[**] The authors thank Dr. R. L. Sutherland for discussions relevant to diffraction theory and Dr. H. Jeon for assistance in obtaining the bright-field TEM images.